JOURNAL OF NEUROTRAUMA 37:1918–1932 (September 1, 2020)

DOI: 10.1089/neu.2019.6738

Neurons in Subcortical Oculomotor Regions Are Vulnerable to Plasma Membrane Damage after Repetitive Diffuse Traumatic Brain Injury in Swine

Carolyn E. Keating,[1,2] Kevin D. Browne,[1,2] John E. Duda,[1,3] and D. Kacy Cullen[1,2,4]

Abstract

Oculomotor deficits, such as insufficiencies in accommodation, convergence, and saccades, are common following traumatic brain injury (TBI). Previous studies in patients with mild TBI attributed these deficits to insufficient activation of subcortical oculomotor nuclei, although the exact mechanism is unknown. A possible cause for neuronal dysfunction in these regions is biomechanically induced plasma membrane permeability. We used our established porcine model of head rotational TBI to investigate whether cell permeability changes occurred in subcortical oculomotor areas following single or repetitive TBI, with repetitive injuries separated by 15 min, 3 days, or 7 days. Swine were subjected to sham conditions or head rotational acceleration in the sagittal plane using a HYGE pneumatic actuator. Two hours prior to the final injury, the cell-impermeant dye Lucifer Yellow was injected into the ventricles to diffuse throughout the interstitial space to assess plasmalemmal permeability. Animals were sacrificed 15 min after the final injury for immunohistological analysis. Brain regions examined for cell membrane permeability included caudate, substantia nigra pars reticulata, superior colliculus, and cranial nerve oculomotor nuclei. We found that the distribution of permeabilized neurons varied depending on the number and spacing of injuries. Repetitive injuries separated by 15 min or 3 days resulted in the most permeability. Many permeabilized cells lost neuron-specific nuclear protein reactivity, although no neuronal loss occurred acutely after injury. Microglia contacted and appeared to begin phagocytosing permeabilized neurons in repetitively injured animals. These pathologies within oculomotor areas may mediate transient dysfunction and/or degeneration that may contribute to oculomotor deficits following diffuse TBI.

Keywords: microglia; NeuN; oculomotor; permeability; TBI

Introduction

Oculomotor deficits are a common occurrence following traumatic brain injury (TBI). Up to 90% of individuals with TBI experience some sort of oculomotor dysfunction, with insufficiencies in accommodation (41%), vergence (56%), and versional movements such as saccades and smooth pursuit (51%) being the most frequent.[1] Similarly, a retrospective study of 50 veterans with non-blast-related TBI found that 90% of patients experienced oculomotor deficits, including 85% who displayed saccadic dysfunction and 62% with accommodation defects.[2] Previous work in patients with mild TBI attributed deficits in saccades and vergence to insufficient activation of subcortical oculomotor nuclei, such as the lateral geniculate nucleus, superior colliculus, cranial nerve nuclei III and IV, and supra-oculomotor area.[3] However, the exact mechanism for this dysfunction is unknown.

A possible underlying cause for neuronal dysfunction in these oculomotor regions may be transient biomechanically induced plasma membrane permeability. These micro- or nano-tears in the plasma membrane are immediate physical consequences of the supra-threshold loading experienced by cells during TBI.[4–9] This so-called ''mechanoporation'' can cause loss of membrane charge, disruption of electrokinetic transport, osmotic imbalance, and loss of calcium homeostasis, ultimately triggering disruption of normal cell function.[5,10–13] Importantly, these acute permeability changes are often transient,[5,8,14] and studies suggest that many initially compromised cells survive the insult but may exhibit later functional alterations[7,15] or protracted cell death.[16]

Delayed cellular dysfunction and death may contribute to the long-term and progressive changes in mood, behavior, and neurological function that are sometimes observed after repetitive mild injuries.[17] In athletes and military veterans in particular, repetitive mild TBI has been linked to neurodegenerative diseases such as

[1]Center for Neurotrauma, Neurodegeneration and Restoration, Corporal Michael J. Crescenz Veterans Affairs Medical Center, Philadelphia, Pennsylvania, USA.
[2]Department of Neurosurgery, [3]Department of Neurology, [4]Department of Bioengineering, University of Pennsylvania, Philadelphia, Pennsylvania, USA.

chronic traumatic encephalopathy, Alzheimer's disease, Parkinson's disease, and various other dementias.[18–23] Due to the consequences of receiving multiple TBIs and the prevalence of oculomotor dysfunction after TBI, we sought to examine the impact of repetitive injuries on the oculomotor system.

The oculomotor system, and saccadic movements in particular, provides an eloquent circuit to investigate the systems-level consequences of TBI. Saccades are originally driven mainly from cortical regions including frontal eye fields, lateral intraperitoneal area, and supplementary eye fields. These areas project to subcortical structures including the caudate and superior colliculus (SC).[24] The caudate receives visually related cortical projections throughout discrete subregions referred to as the head, body, and tail, with oculomotor-specific neurons located in the head and body subregions.[25] The caudate then sends an inhibitory projection to the substantia nigra pars reticulata (SNpr), a key output region of the basal ganglia. The SNpr, whose projection neurons are also GABAergic, tonically inhibits firing of the SC. When an eye movement is to be made, the caudate inhibits the SNpr, thus disinhibiting the SC. The SC is then able to activate brainstem regions which in turn stimulate the cranial nerve nuclei that control the eye muscles.[24]

To investigate damage to the oculomotor system resulting from TBI, we used a porcine model of closed-head rotational acceleration.[26,27] This well-characterized model subjects the head to rapid angular acceleration, inducing inertial forces common in human TBI resulting from falls, collisions, or blunt impacts. Because of this ability to replicate the injury biomechanics seen in humans—owing to neuroanatomical features of swine such as large, gyrencephalic brains with a gray-to-white matter ratio similar to humans[28-30]—this model has been shown to produce acute and chronic pathologies in swine in patterns and extents that mirror those seen clinically.[31-33]

Using this swine model of closed-head rotational acceleration, we have observed acute plasmalemmal disruptions of neurons accompanied by an increase in microglia density in close proximity to those neurons after single injuries in the cerebral cortex and hippocampus.[34] Building on these findings, we predicted that neuronal populations in subcortical structures involved with oculomotor function would also exhibit plasma membrane damage following diffuse TBI, particularly after repetitive injuries. We also assessed changes in neuronal loss, neuron-specific nuclear protein (NeuN) reactivity, and microglia. This neuronal plasma membrane permeability and subsequent evolving neuropathology could underlie the dysfunction that contributes to oculomotor deficits following injury.

Methods

Animal care and anesthesia

All procedures and protocols were approved by the Animal Care and Use Committee of the University of Pennsylvania. All animal care complied with the Guide for the Care and Use of Laboratory Animals. Female Yorkshire swine ($n = 23$) between 2-3 months of age and weighing 20-30 kg were used. Animals were housed indoors with access to normal feed and water *ad libitum.* The housing facility was accredited by the Association for Assessment and Accreditation of Laboratory Animal Care International. Prior to the injection and/or injury procedure, animals were fasted for 18-20 h with water remaining *ad libitum.* After induction with a cocktail of ketamine (20-30 mg/kg; Hospira, Lake Forest, IL) and midazolam (0.4-0.6 mg/kg; Hospira, Lake Forest, IL), anesthesia was provided with 5% isoflurane (Akorn Inc., Lake Forest, IL) via a snout mask, and glycopyrrolate (0.01 mg/kg; West-Ward Pharmaceuticals, Eatontown, NJ) was given subcutaneously to reduce secretions. The animal was then intubated, and isoflurane was connected at maintenance levels (1.5-2.0%). Eye lubricant was used to minimize drying. Physiological monitoring allowed titration of anesthesia so that SpO_2, heart rate, and respirations were within acceptable ranges.

Delivery of Lucifer Yellow via intracerebroventricular injections

As described previously,[34] Lucifer Yellow (LY; Invitrogen, Carlsbad, CA)—an aldehyde-fixable, cell-impermeable dye—was delivered into the lateral ventricles of all animals before the rotational or sham injury to label cells permeabilized during the injury. Animals were placed in a stereotactic head frame and a 7 cm incision was made in the scalp. The scalp was reflected from the skull in order to visualize bregma. Two 5 mm craniectomies were made at the following stereotactic coordinates: 1.0 mm posterior to bregma, ±6.0 mm lateral. A small incision in the dura was made with a 19-gauge needle. For each site in serial fashion, a Hamilton syringe (Reno, NV) was lowered 18.0 mm from the surface of the dura mater to access the ventricles. The brain was left to stabilize for 2 min before delivering 500 μL of LY (10 mg/mL in sterile saline) per side over a period of 10 min per injection using an UltraMicroPump III (World Precision Instruments, Sarasota, FL). The needle was slowly withdrawn and the burr holes were sealed with bone wax. The incision site was closed with 0-0 sutures. A surgical plane of anesthesia was maintained through the injury/sham procedure and sacrifice. The injury occurred 2 h after the start of the first injection to allow LY to evenly distribute throughout the brain tissue. For animals receiving repetitive injuries separated by 3 or 7 days, LY injection occurred prior to the second injury only.

Porcine closed-head rotational/inertial TBI

Briefly, animals were anesthetized and subjected to rapid head rotational acceleration in the sagittal plane using a HYGE pneumatic actuator. Angular velocity was recorded using a magneto-hydrodynamic sensor (Applied Technology Associates, Albuquerque, NM) connected to a National Instruments DAQ, controlled by LabVIEW. The anesthetized animal's head was secured to a padded bite plate and mounted to the HYGE device. Head rotation in the sagittal plane occurred at mean peak angular velocities of 102 ± 11 radians/sec, with most rotations corresponding to a ''moderate'' injury level based on the clinically defined time of neurological recovery.[27] Animals received single rotations ($n = 5$-7), or repetitive rotations separated by 15 min ($n = 4$), 3 days ($n = 4$), or 7 days ($n = 3$-4). Sham animals ($n = 4$) received all other procedures absent head rotation.

Brain tissue acquisition and processing

All animals were sacrificed within 15 min of head rotational injury (15 min following the second injury for the animals subjected to repetitive head rotations). Animals were transcardially perfused using heparinized saline (4°C, 2-3 L) followed by chilled 4% paraformaldehyde (4°C, 8-10 L; Sigma, St. Louis, MO). Brains were blocked in the coronal plane at 5 mm intervals and transferred to 30% sucrose until saturated. The blocks then were placed in OCT, flash frozen in isopentane (Fisher Scientific, Waltham, MA), and stored at -80°C. Twenty micron-thick sections were cut coronally on a cryostat (Leica Biosystems, Buffalo Grove, IL).

Additional age-matched, naïve female Yorkshire swine ($n = 3$) were used for a brain atlas and neuronal phenotype determination. Animals were transcardially perfused using heparinized saline (4°C, 2-3 L) followed by 10% neutral buffered formalin (8-10 L;

Sigma, St. Louis, MO). Brains were blocked in the coronal plane at 5 mm intervals and process through paraffin. Eight-micron thick sections were cut coronally on a microtome (Thermo Scientific, Waltham, MA).

Immunohistochemistry and imaging

Florescent immunohistochemistry on paraformaldehyde-fixed frozen sections was performed with several antibodies against neuronal-type specific markers to aid in anatomical identification, as well as antibodies for pathological assessments: tyrosine hydroxylase (TH; sheep 1:1000, Abcam, Cambridge, MA), parvalbumin (PV; rabbit 1:250, Abcam), choline acetyltransferase (ChAT; goat 1:500, Millipore, Burlington, MA), NeuN (mouse 1:500, Millipore), and/or ionized calcium binding adaptor molecule 1 (Iba1; rabbit 1:1000, Wako, Richmond, VA). Mounted sections were washed in phosphate buffered saline (PBS) and blocked in 4% normal horse serum (NHS; Sigma, St. Louis, MO) with 0.3% Triton X-100 (Sigma, St. Louis, MO) for 1 h at room temperature. Slices were incubated with primary antibody in blocking solution overnight at 4°C. Secondary antibodies were applied at a 1:1000 concentration for 2 h at room temperature in blocking solution: donkey anti-sheep 647 (Jackson Immuno, West Grove, PA), donkey anti-rabbit 568 (Invitrogen), donkey anti-rabbit 647 (Invitrogen), donkey anti-goat 568 (Invitrogen), donkey anti-mouse 647 (Life Technologies, Carlsbad, CA) goat anti-mouse IgG1 555 (Invitrogen). Sections were counterstained with Hoechst (Hoechst 33342, Life Technologies, Carlsbad, CA) or Neurotrace 435/455 Blue Fluorescent Nissl stain (ThermoFisher, Waltham, MA) before being cover-slipped with Fluoromount-G (Southern Biotech, Birmingham, AL).

To counterstain with fluorescent Nissl, tissue was washed in PBS before being permeabilized with 0.1% Triton-X for 10 min. Neurotrace 435/455 Blue Fluorescent Nissl stain was applied for 20 min at a concentration of 1:100 in PBS. Slides were washed briefly in PBS +0.1% Triton before incubating in PBS for either 2 h at room temperature or overnight at 4°C. Sections were cover-slipped with Fluoromount-G.

Because injured cells can lose their antigenicity for certain neuronal markers,[35-37] formalin-fixed paraffin-embedded tissue from age-matched naïve female Yorkshire swine was used in order to obtain representative fluorescent images of cell phenotypes in the various oculomotor regions examined for a Yorkshire brain atlas. The same antibodies were used as described for paraformaldehyde-fixed frozen sections, with the following concentrations: TH 1:500; PV 1:1000; NeuN 1:1000; ChAT 1:250. Slides were dewaxed in citrosolv (Fisher Scientific) and rehydrated in ethanol and de-ionized water. Antigen retrieval was completed in Tris-EDTA buffer pH 8.0 (Sigma, St. Louis, MO) using a microwave pressure cooker. Tissue was blocked in Optimax buffer (Fisher Scientific) plus NHS for 30 min at room temperature. Primary antibodies were diluted in Optimax and incubated overnight at 4°C. Slides were washed with PBS-Tween (Sigma, St. Louis, MO) before incubation with secondary antibodies (same concentrations as frozen sections) in Optimax plus NHS for 1 h at room temperature. Slides were cover-slipped with Fluoromount-G.

Hematoxylin and eosin (H&E) staining was performed on formalin-fixed paraffin embedded-tissue (as well as one block of sham frozen tissue) to contribute to a Yorkshire brain atlas. Slides were dewaxed in xylene (Fisher Scientific) and rehydrated in ethanol and de-ionized water. Nuclei were stained with Mayer's Hematoxylin (Fisher Scientific) and blued with lithium carbonate (Sigma, St. Louis, MO). Tissue was counterstained with eosin (Fisher Scientific). Eosin was differentiated and slides were dehydrated in ethanol before being cleared in xylene and cover-slipped with Cytoseal (Fisher Scientific).

Fluorescence images used for quantification were acquired with an Eclipse Ni-E (Nikon, Tokyo, Japan) upright fluorescent microscope or Keyence BZ-X800 (Keyence, Osaka, Japan) fluorescent microscope. Publication-quality representative images were taken on either a confocal microscope (A1RSI Laser Scanning Confocal; Nikon) using 10×, 20×, or 60× objectives with or without 2× optical zoom, or Keyence microscope using a 20× objective. Examination of H&E sections was performed using light microscopy on an Eclipse E600 (Nikon) and images were acquired using an Aperio Scanscope CS2 (Leica Biosystems, Buffalo Grove, IL).

Quantification

All quantification was conducted by a skilled scientist who was blinded as to the tissue experimental group. LY+ cells were manually quantified from slides cut from 2-3 different blocks of tissue per anatomical region of interest (ROI) per animal, except for a few cases when only one block was available.

To put the number of permeabilized cells per ROI in context with the total number of neurons per ROI in one tissue section, the number of Nissl+ cells was also quantified for each animal. As the SC and caudate are large regions with many cells, Nissl+ cells in these ROIs were quantified semi-automatically using the Pixel Classification workflow of ilastik software.[38] Briefly, the software was trained to recognize Nissl+ cells from background using training images before images of entire ROIs were batch processed. The resulting simple segmentation map was exported as a TIF file and opened in FIJI. A size threshold of 50-1000 μm^2 and circularity range of 0.25-1.00 were used to restrain the particle analysis. Nissl+ cells in SN and oculomotor nuclei were quantified by hand as these regions are either sparsely populated or small in area, respectively.

The number of LY+ cells was then put in context with the number of Nissl+ cells per ROI, and is expressed as the percentage of LY+ Nissl cells per hemisphere, ± standard error of the mean (SEM).

The number of NeuN+ cells in each ROI also was assessed as a marker of neuronal injury. NeuN was quantified as described above for the Nissl staining, though using a size threshold of 80-800 μm_2. Similar to LY, the number of NeuN+ cells was expressed as a percentage of Nissl cells per hemisphere. Additionally, the number of LY+ cells that were NeuN+ was quantified by hand for each ROI, and expressed at the percentage of NeuN+ LY cells per hemisphere.

Microglia reactivity was assessed by examining the density and intensity of Iba1 in each ROI. Density was quantified by semi-automatically using ilastik software to identify microglia cell bodies. The resulting simple segmentation map was opened in FIJI, where particles with a minimum size of 20 μm^2 were counted, and expressed as the number of Iba1+ cells per mm^2. FIJI also was used to take Iba1 fluorescence intensity measurements of the entire ROI, as well as several background (Iba1-) regions within the ROI. Iba1 intensity is expressed as $\frac{\text{Intensity} - \text{Background}}{\text{Background}}$. We also noticed large clusters of Iba1+ cells that appeared to contain small LY+ particles. Cells displaying this colocalization were counted by hand and expressed as the number of Iba1+/LY+ cells per mm^2.

Statistical analysis

Percentage data within a range of 0-20% or data without a normal distribution was log transformed using the equation $Y = \log(Y + 1)$ before further statistical analyses. To detect statistical differences between groups, one-way analyses of variance (ANOVAs) with Tukey's multiple comparisons tests were performed. When data distribution assumptions for ANOVA were not met, Kruskal-Wallis non-parametric tests with Dunn's multiple comparisons tests were used. The p values are reported as follows: non-significant $p > 0.05$, $*p \leq 0.05$, $**p \leq 0.01$, $***p \leq 0.001$, $****p \leq 0.0001$.

Post hoc analyses revealed that the study was adequately powered to detect permeability differences between groups for each region examined except the oculomotor nuclei in which tissue from

fewer animals was available (caudate: power = 0.913, effect size $f = 0.983$; SNpr: power = 0.874, effect size $f = 0.956$; SC: power = 0.991, effect size $f = 1.247$; oculomotor nuclei [CNIII/IV]: power = 0.684, effect size $f = 0.799$). The study also was adequately powered to detect differences in Iba1 and LY colocalization for each region except the caudate (caudate: power = 0.719, effect size $f = 0.753$; SNpr: power = 0.930, effect size $f = 1.047$; SC: power = 0.854, effect size $f = 0.931$; CNIII/IV: power = 0.997, effect size $f = 1.723$). It also was adequately powered to detect differences between the percentages of LY+/NeuN- between injury groups in all regions examined except the SNpr (caudate: power = 0.949, effect size $f = 0.945$; SNpr: power = 0.555, effect size $f = 0.677$; SC: power = 0.985, effect size $f = 1.233$).

Results

To investigate TBI-induced neuronal plasma membrane permeability, we used a porcine model of closed-head rotational acceleration (Fig. 1). Swine were subjected to sham conditions or head rotational acceleration in the sagittal plane using a HYGE pneumatic actuator. Rotational injuries were either single or repetitive, with repetitive injuries separated by 15 min (0d), 3 days (3d), or 7 days (7d). Two hours prior to the final injury, the normally cell-impermeant dye Lucifer Yellow (LY) was injected into the ventricles to diffuse throughout the interstitial space. In this way, cells experiencing plasmalemmal permeability during injury would be labeled with the dye. Animals were sacrificed 15 min after the final injury for immunohistological analysis. Several subcortical brain regions involved in oculomotor functions were examined for neuronal permeability (Fig. 2). In particular, we focused our analysis on regions involved in saccadic eye movements. Specifically, we analyzed tissue slices from the caudate, SNpr, SC, and cranial nerve nuclei III and IV (oculomotor and trochlear, respectively, here referred to together as CNIII/IV). Permeabilized cells were exclusively neuronal, as described previously[34] and as shown by Nissl staining (Supplementary Fig. S1). The number of permeabilized neurons in each region was put in context with the number of Nissl+ cells per region.

Acute neuronal permeability

In the head and head-to-body transition of the caudate, permeabilized cells were relatively infrequent. LY+ cells were generally scattered throughout the structure, although sometimes cells were found concentrated in clusters, particularly in the most dorsolateral region (Fig. 3A-E, 3G, 3H). However, one 3d repetitive animal was unusual in that instead of a few intensely-labeled permeabilized cells, there were many faintly labeled cells concentrated predominantly in the ventral portion of the structure.

The distribution of permeabilized cells is important, as visual- and oculomotor-related neurons are found throughout the head, body, and tail of the caudate.[25] Although in macaques saccade-related neurons were predominantly found in dorsomedial regions where the head of the caudate transitions into the body,[39] studies in macaque and cat have demonstrated that both the frontal and

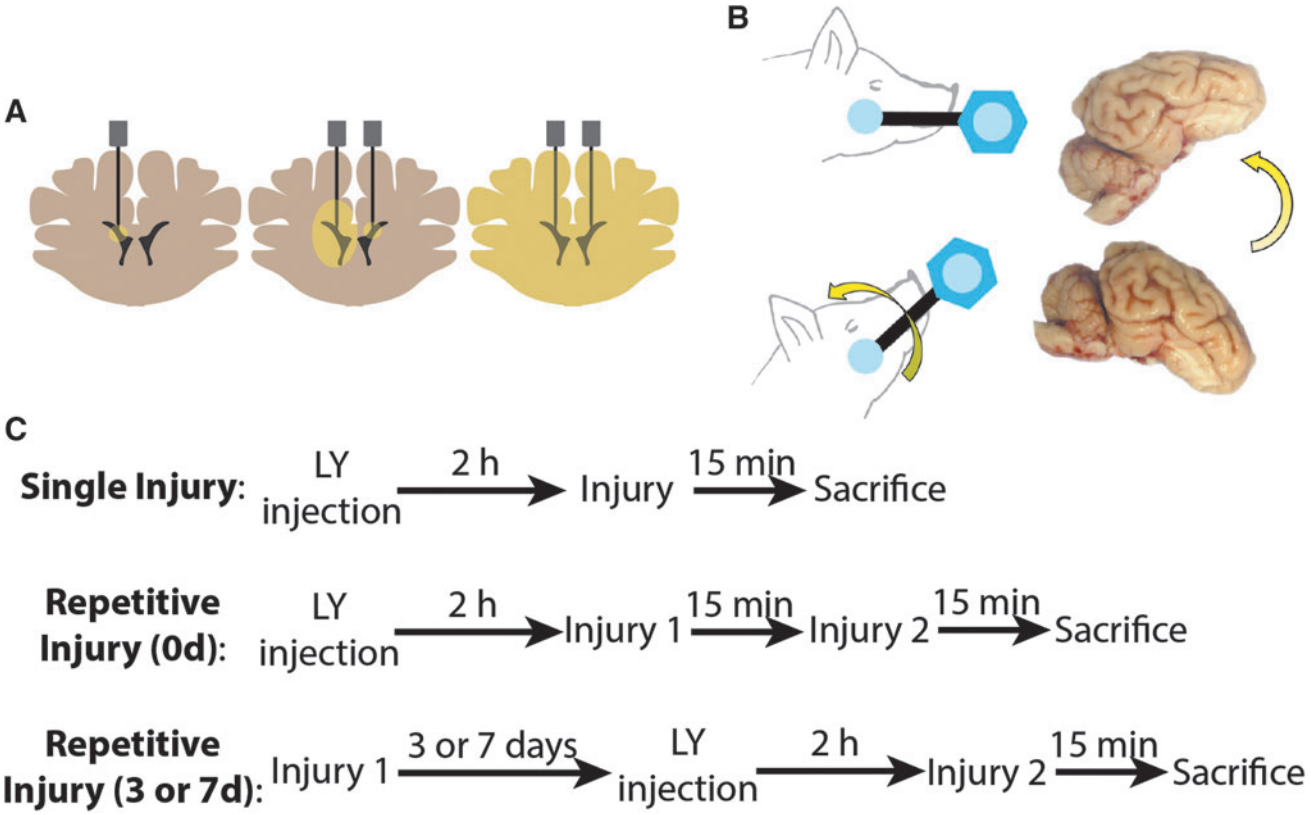

FIG. 1. Experimental overview. **(A)** Schematic of Lucifer Yellow (LY) intracerebroventricular injections. Bilateral craniectomies were made at the approximate brain level shown. Needles were lowered into the ventricles. LY was delivered sequentially on each side and allowed to diffuse throughout the parenchyma. **(B)** Anesthetized swine were subjected to rapid head rotational acceleration in the sagittal plane using a HYGE pneumatic actuator. **(C)** Experimental timeline for single and repetitive injuries (same day and separated by 3 or 7 days). Note that animals receive LY injections on the second injury day for 3- and 7-day repetitive groups, and all animals are sacrificed at 15 min post-final injury. Color image is available online.

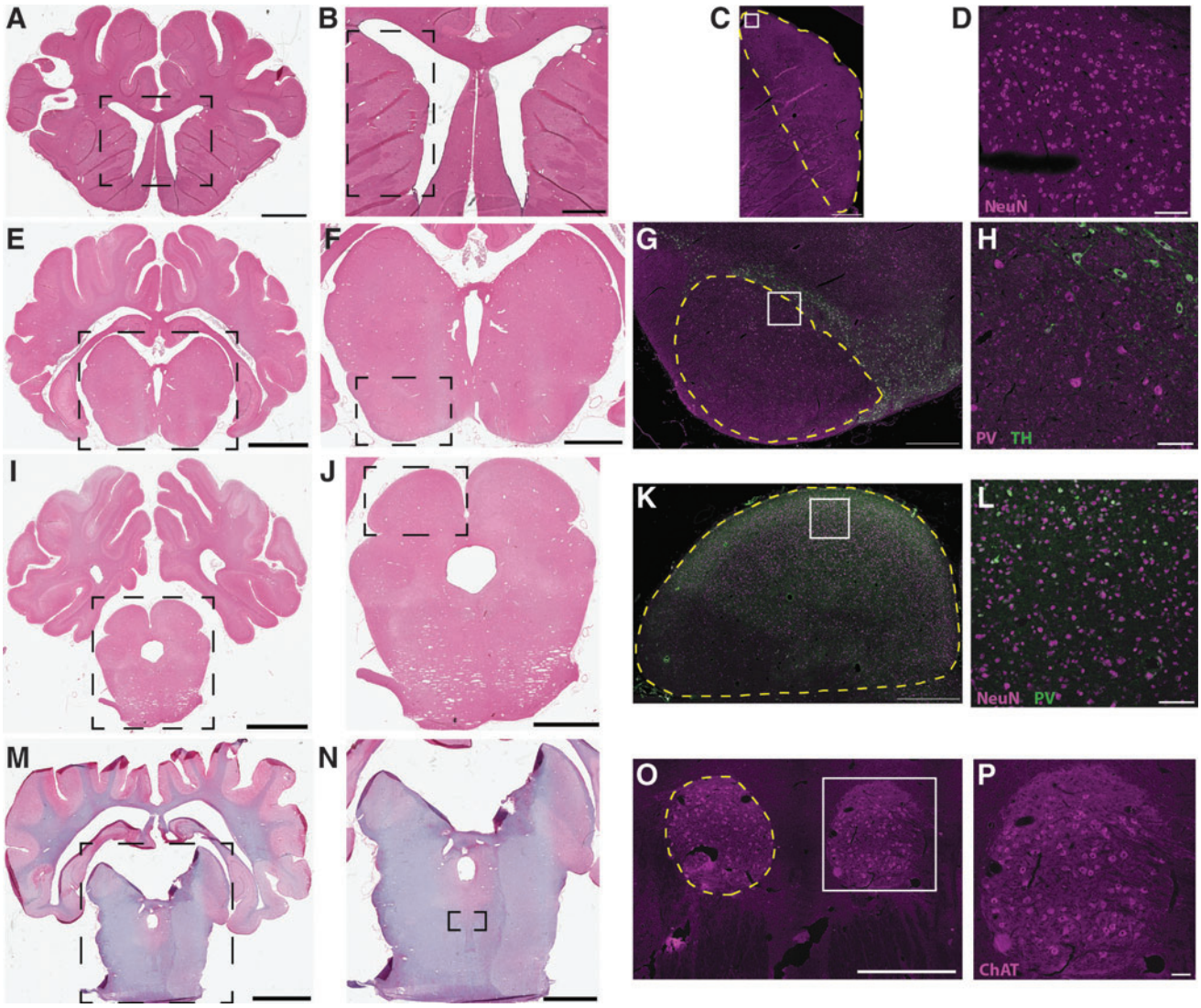

FIG. 2. Swine oculomotor neuroanatomy. Representative blocks showing caudate **(A-D),** substantia nigra **(E-H),** superior colliculus **(I-L),** and oculomotor cranial nerve nuclei **(M-P)**. Hematoxylin and eosin panels on left illustrate gross structure, while fluorescent panels of adjacent sections illustrate cell phenotypes. (C, D) Neuron-specific nuclear protein (NeuN), a neuronal marker, purple. (G, H) Tyrosine hydroxylase (TH), a marker of dopaminergic neurons in the pars compacta, green; parvalbumin (PV), a marker of inhibitory neurons in the pars reticulata, purple. (K, L) PV, a marker of inhibitory neurons found in superficial layers, green; NeuN, purple. (O, P) Choline acetyltransferase (ChAT), a marker of motorneurons, purple. Boxes indicate magnified areas in the following panel. Dashed yellow lines indicate boundaries of anatomical regions of interest. Scale bars: (A) 5 mm, (E, I) 8 mm, (M) 9 mm, (B) 2 mm, (F, J) 4 mm, (N) 5 mm, (C, G, K, O) 1 mm, (D, H, L, P) 100 μm. Color image is available online.

supplemental eye fields, as well as other extrastriate visual areas, project to the dorsolateral region.[40-42] Further, tracing studies have shown that caudate neurons in the dorsolateral region project to the SNpr.[43] However, as the caudate is involved in many functions, it is possible that the permeabilized neurons are not related to oculomotor tasks. Overall, it appeared that more permeabilized neurons were present in 3d repetitive animals, and to a lesser extent in 0d repetitive animals, whereas sham, single, and 7d repetitive injuries had even fewer permeabilized cells. Kruskal-Wallis nonparametric ANOVA revealed that this trend was nearly significant ($p=0.0567$; Fig. 3F).

In the SNpr, many permeabilized cells were found in 0d and 3d repetitive injuries (Fig. 4A-E). Quantification revealed that over 50% of neurons were permeabilized in these groups (Fig. 4F). In contrast, sham, single, and 7d repetitive injuries all had similarly low numbers of permeabilized cells. One-way ANOVA revealed significant differences between groups ($p=0.0084$). Multiple comparisons demonstrated that sham injuries were statistically different from 0d repetitive ($p=0.0281$) and 3d repetitive injuries ($p=0.0419$). Single injuries were trending towards being statistically different from the 0d repetitive group as well ($p=0.0849$).

In the SC, very few of the total number of neurons in each tissue section were permeabilized. Nevertheless, the same pattern was seen in this region as in the previous two areas, with 0d and 3d repetitive injuries exhibiting more permeabilized neurons compared with sham, single, and 7d repetitive injuries (Fig. 5A-E). One-way ANOVA showed significant differences between groups ($p=0.0011$), with 0d repetitive injuries producing more permeabilized cells than sham ($p=0.0063$), single ($p=0.0054$), and

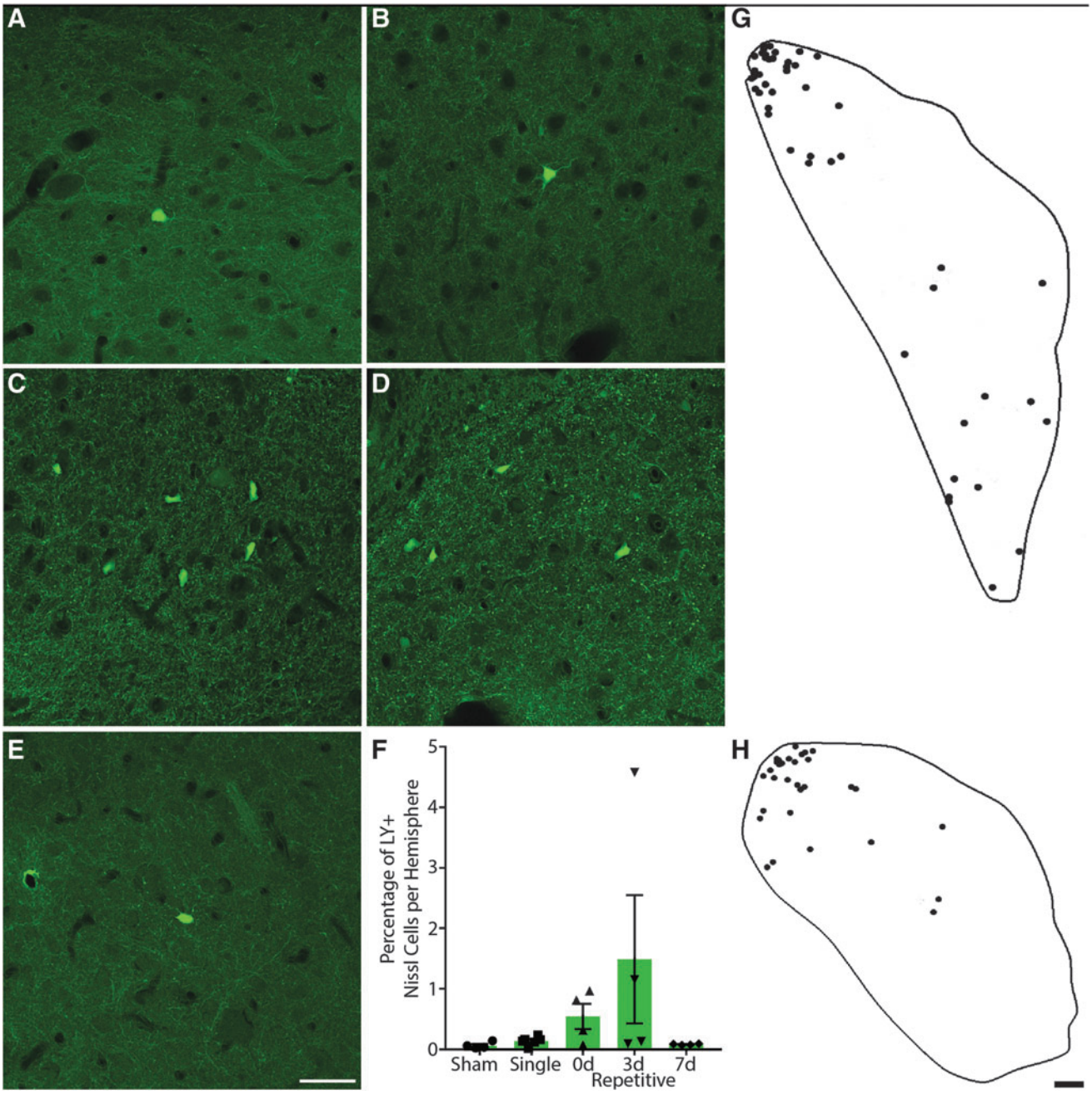

FIG. 3. Neuronal permeability in the caudate. Representative images of regions from **(A)** sham, **(B)** single, **(C)** 15-min (0d) repetitive, **(D)** 3-day (3d) repetitive, and **(E)** 7-day (7d) repetitive injuries. Lucifer Yellow (LY), green. Scale bar = 50 μm. **(F)** Quantification of LY permeability as a percentage of Nissl+ cells per hemisphere, ± standard error of the mean. Though not quite statistically significant ($p = 0.0567$), permeability is increased in animals injured repetitively 3 days apart and to a lesser extent in animals injured 15 min apart. **(G and H)** Tracings depicting regional distribution of permeabilized cells (dots) within (G) the head of the caudate in a 0d repetitive injury and (H) the head to body transition of the caudate in a 3d repetitive injury. Permeabilized cells are located in regions involved with oculomotor functions. Scale bar = 500 μm. Color image is available online.

7d repetitive ($p = 0.0043$) injuries (Fig. 5F). Additionally, permeabilized cells tended to be distributed in intermediate and deep layers, as opposed to superficial layers of the SC (Fig. 5H). This localization is noteworthy, as these intermediate and deep layers are the regions that receive input from the SNpr and are involved in saccade generation.[44] What appeared to be neuritic beading also was occasionally observed in the intermediate and deep layers of 0d and 3d repetitive injuries (Fig. 5G).

The CNIII/IV complex was difficult to delineate in some animals depending on how the tissue was initially cut during blocking, which led to fewer animals analyzed per group: sham $n = 3$, single $n = 5$, 0d repetitive $n = 3$, 3d repetitive $n = 4$, 7d repetitive $n = 3$. In CNIII/IV a few permeabilized neurons were found in most animals, with no permeabilized cells seen in 7d repetitive injuries (Fig. 6A-E). Animals injured repetitively 3 days apart appeared to have the most permeabilized cells, although one-way ANOVA showed that

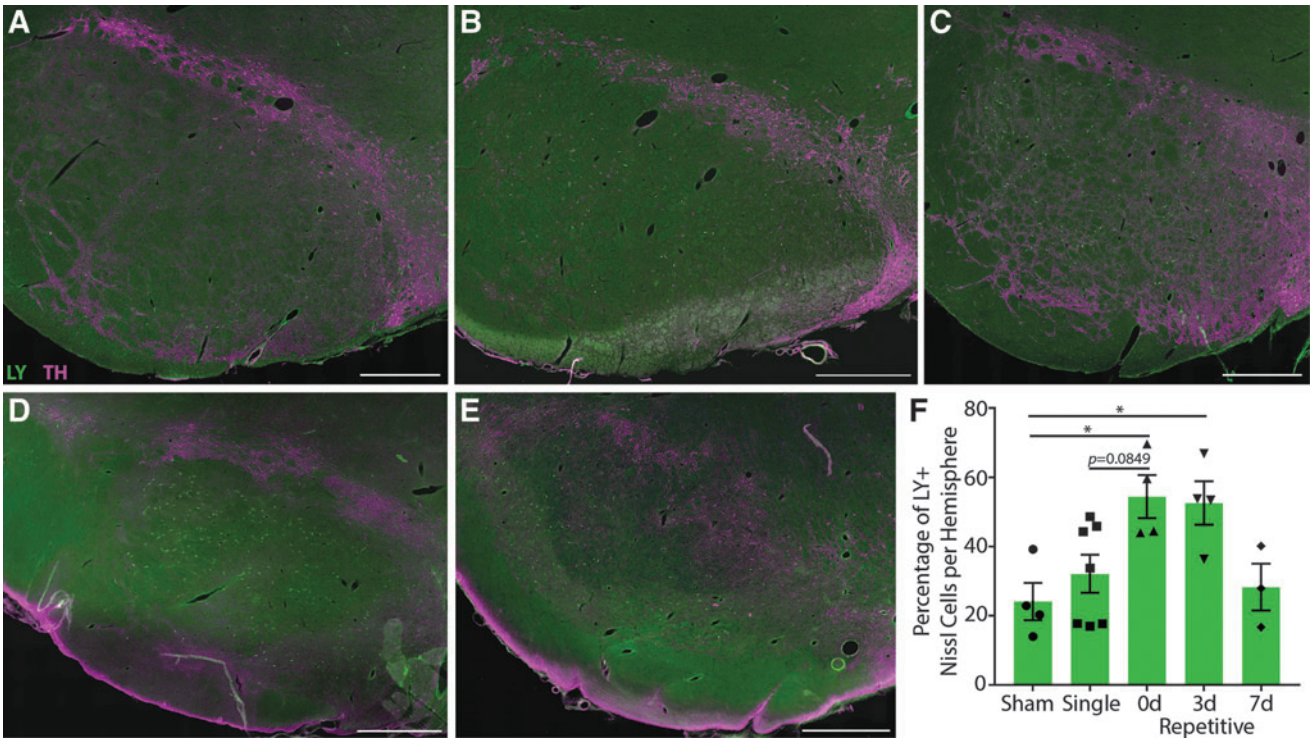

FIG. 4. Neuronal permeability in the substantia nigra pars reticulata. Representative images from **(A)** sham, **(B)** single, **(C)** 15-min (0d) repetitive, **(D)** 3-day (3d) repetitive, and **(E)** 7-day (7d) repetitive injuries. Lucifer Yellow (LY), green; TH, purple. Scale bars = 1 mm. (F) Quantification of LY permeability as a percentage of Nissl+ cells per hemisphere, ± standard error of the mean. There were significant differences in permeability between groups ($p = 0.0084$), with the most permeability in animals injured repetitively 15 min and 3 days apart. Color image is available online.

there were no significant differences between any groups ($p = 0.0786$; Fig. 6F), possibly due to the low number of cases analyzed.

Acute neuropathological changes

In addition to assessing plasma membrane permeability, we investigated several other pathologies in these oculomotor regions. To examine cell loss, the number of Nissl+ cells was quantified (Fig. 7). There were no differences in neuronal loss in any region (caudate $p = 0.0690$; SNpr $p = 0.7609$; SC $p = 0.6828$; CNIII/IV $p = 0.9862$). This finding is not surprising, as animals were sacrificed just 15 min after the final injury. However, it suggests that there was no cell death as a consequence of the first injury (i.e., either 3 or 7 days prior in this cohort) at this rotational severity.

Another marker often used to measure cell loss is NeuN, though lack of NeuN signal can instead reflect loss of antigenicity as opposed to cell loss, and has been suggested to predict delayed neuronal degeneration.[36,37] We observed no differences in overall percentage of NeuN+ Nissl cells among injury groups in any region (Supplementary Fig. S2), though CNIII/IV was not analyzed as there was not enough remaining tissue to perform meaningful statistics. However, we noticed that permeabilized neurons in particular displayed altered NeuN staining, in some cases expressing NeuN very weakly and in others not at all (Fig. 8A). Quantification of the percentage of LY+ neurons co-expressing NeuN revealed that only 42.46% of permeabilized neurons were NeuN+ in the caudate, while 92.49% of LY+ neurons in the SN and 64.48% of permeabilized cells in the SC were NeuN+ (Fig. 8B-D). It is possible that this loss of NeuN in permeabilized neurons was not reflected in a loss of total NeuN due to relatively low numbers of permeabilized cells in certain areas like the caudate. There were no differences in the percentage of NeuN+ permeabilized neurons between each group (caudate $p = 0.2861$; SNpr $p = 0.0636$; SC $p = 0.9267$).

However, as 0d and 3d repetitively injured animals have more LY+ cells, any consequences of NeuN loss may be more apparent in these animals as opposed to other injury conditions where the number of permeabilized neurons is much lower. Indeed, an examination of the percentage of LY+ neurons that did not express NeuN (Fig. 8E-G) revealed that there were significant differences between injury groups in the caudate ($p = 0.0379$) and SC ($p = 0.0202$), but this significance was lost in Dunn's non-parametric multiple comparison analyses. In contrast, there were no differences in the percentage of LY+/NeuN- neurons in the SNpr ($p = 0.1762$).

To investigate acute inflammatory changes in oculomotor areas, we assessed microglia reactivity. While the overall density and intensity of Iba1 staining were not different across injury groups in any region (Supplementary Fig. S3), microglia were seen interacting with LY+ neurons (Fig. 9A). In some cases, large clusters of microglia were observed with LY+/Nissl+ signal inside of them, suggesting phagocytosis of acutely permeabilized neurons (Fig. 9B). Quantification of large Iba1+ signal containing LY revealed that this colocalization occurred most often in repetitively injured animals, particularly those injured 3 days apart (Fig. 9C-F). This pattern was most evident in the SC ($p = 0.0273$), with animals injured repetitively 3 days apart displaying more Iba1/LY colocalization compared with single ($p = 0.0324$) and to a lesser extent sham ($p = 0.0512$) injuries. Colocalization did not reach statistical significance in the other oculomotor regions examined (caudate $p = 0.0680$; SNpr $p = 0.1457$; CNIII/IV $p = 0.2000$), perhaps due to the infrequency and high variability of these events.

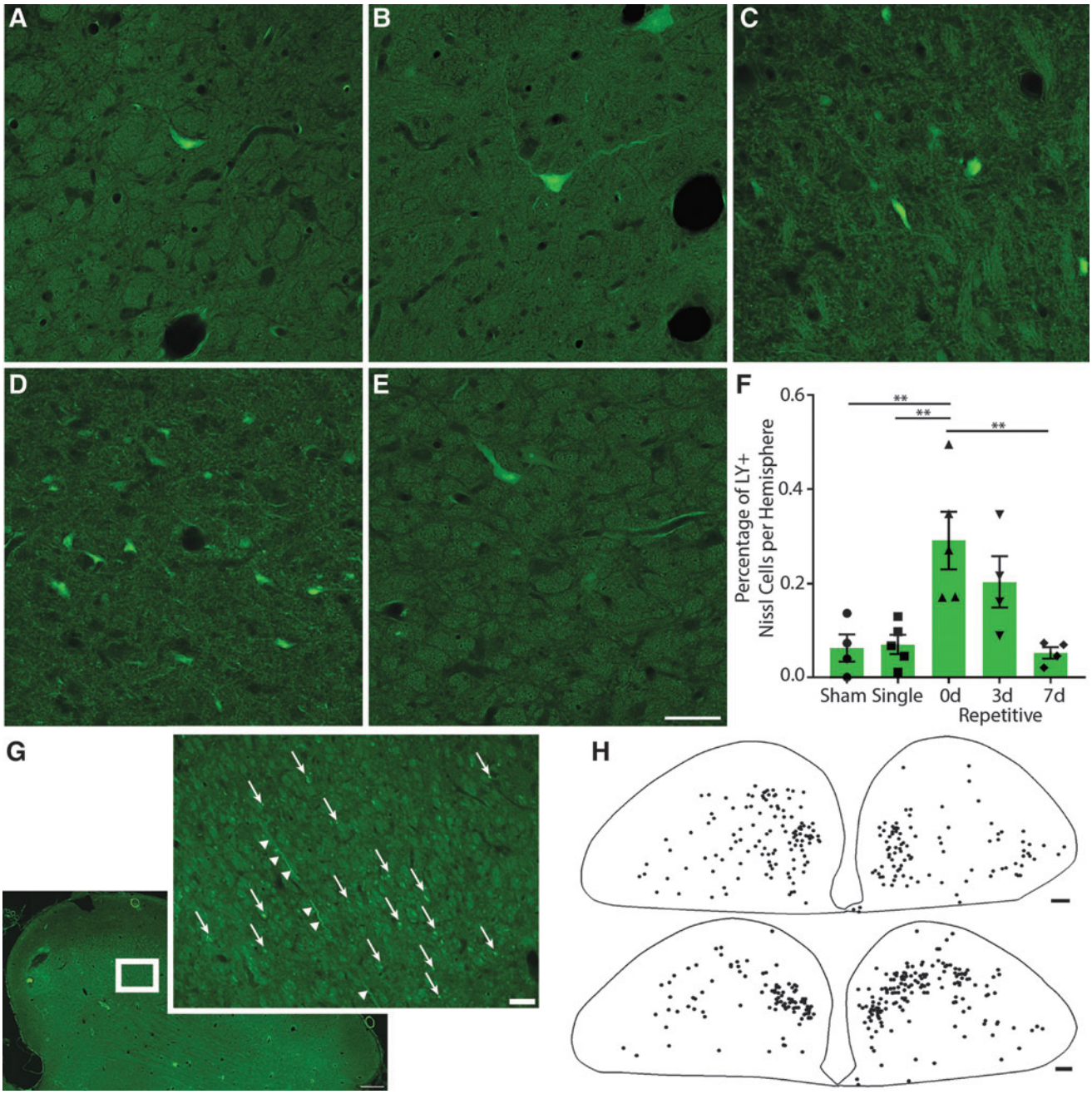

FIG. 5. Neuronal permeability in the superior colliculus. Representative images of regions from **(A)** sham, **(B)** single, **(C)** 15 min (0d) repetitive, **(D)** 3-day (3d) repetitive, and **(E)** 7-day (7d) repetitive injuries. Lucifer Yellow (LY), green. Scale bar = 50 μm. **(F)** Quantification of LY permeability as a percentage of Nissl+ cells per hemisphere, ± standard error of the mean. There were significant differences in permeability between groups ($p = 0.0011$), with the most permeability in animals injured repetitively 15 min and 3 days apart. **(G)** Example of LY+ neuritic beading in intermediate layer of 0d repetitive injury. LY, green. Box indicates magnified region in inset. Arrows indicate punctate neuritic beading, arrowheads indicate LY+ neuritic process passing through region. Overview scale bar = 500 μm, inset scale bar = 50 μm. (H) Tracings depicting regional distribution of permeabilized cells (dots) within 0d (top) and 3d (bottom) repetitive injuries. Permeabilized cells are located in regions involved with oculomotor functions. Scale bar = 1 mm. Color image is available online.

Discussion

Here, we report for the first time neuronal plasma membrane damage across several brain regions involved with oculomotor function. Permeability was observed predominantly in animals injured repetitively 15 min or 3 days apart. Within large multifunctional regions like the caudate and SC, permeabilized cells were located in subregions responsible for oculomotor activity. However, it should be noted that permeabilized cells were not exclusive to oculomotor regions in this injury model, as we have observed neuronal plasma membrane vulnerability in the cerebral cortex and hippocampus as well.[34] Despite no neuronal loss at this acute time point after injury, we report loss of NeuN reactivity in permeabilized cells, along with observations of microglia that

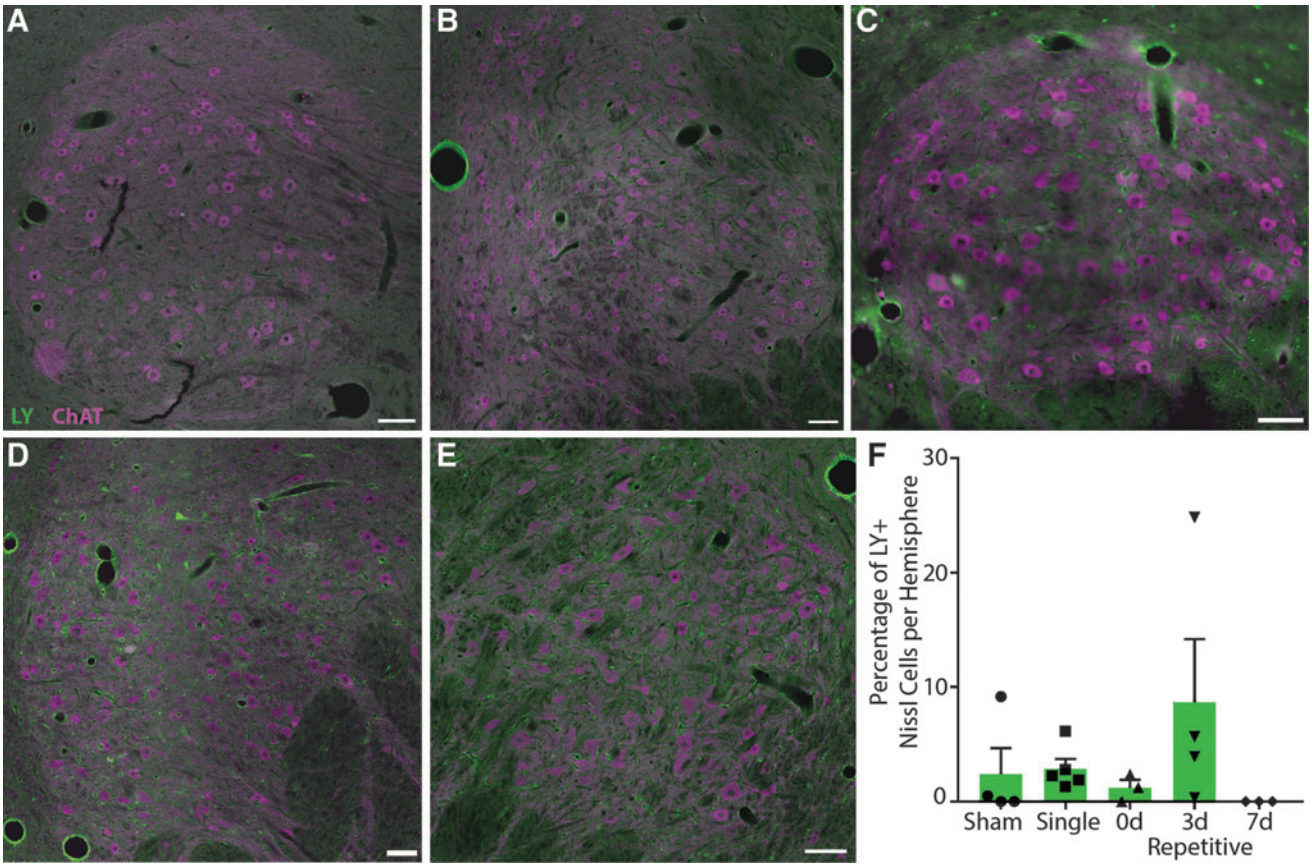

FIG. 6. Neuronal permeability in cranial nerve oculomotor nuclei. Representative images from **(A)** sham, **(B)** single, **(C)** 15 min (0d) repetitive, **(D)** 3-day (3d) repetitive, and **(E)** 7-day (7d) repetitive injuries. Lucifer Yellow (LY), green; ChAT, purple. Scale bars = 100 μm. **(F)** Quantification of LY permeability as a percentage of Nissl+ cells per hemisphere, ± standard error of the mean. Permeability appears to be greatest in animals injured repetitively 3 days apart, though this trend was not significant ($p = 0.0786$). Color image is available online.

appear to be actively phagocytosing permeabilized neurons. These neuronal plasma membrane disruptions and associated pathologies within oculomotor areas may mediate transient dysfunction and/or degeneration that may contribute to the symptomology of oculomotor deficits following diffuse TBI.

It is no surprise that oculomotor dysfunction is common after TBI, as more than half of the circuitry in the brain is implicated in vision. Because there are so many visually-associated brain areas, we chose to limit the number of regions examined. Areas involved in saccades were selected as a focus for several reasons. First, the underlying neural circuitry is well known. The subcortical structures in particular are readily identifiable in the pig (with the exception of the paramedian pontine reticular formation (PPRF), as described in more detail below). In contrast, the cortical structures underlying vision would be difficult to confidently identify purely by histology, especially given the lack of in-depth brain atlases for these animals. Second, saccadic dysfunction is common after TBI in humans. A retrospective study of 50 veterans with non-blast-related TBI found saccadic dysfunction in 85% of patients,[2] while another retrospective study of ambulatory outpatients identified 62 of 160 TBI patients with saccade deficits and 19 of 160 with saccadic intrusions.[1] A more recent meta-analysis found that mild and severe TBI had a significant impact on saccades and smooth pursuit.[45] Finally, saccades are a behavior that could potentially be assessed in swine, which cannot be said of all oculomotor functions known to occur in humans. For instance, although convergence or accommodation insufficiencies may also occur following TBI, the anatomy and physiology of the pig likely prohibits these behaviors: pig' eyes are located fairly laterally, resulting in little binocular vision. Further, they are thought to be unable to accommodate and have poor near vision. For these reasons, we chose to focus on saccades and their subcortical circuitry.

Notably, the PPRF, a crucial mediator of saccade generation, was excluded from this analysis. As mentioned, swine brain neuroanatomy is less well-characterized than that of humans or animals such as primates or rodents. We were not confident in our ability to distinguish the PPRF from surrounding tissue using histology alone, and therefore did not include this region in our analysis. While not quantified, we did observe permeabilized cells in the pons (Fig. 2I, 2J; region below the cerebral aqueduct) of 0d and 3d repetitively injured animals (data not shown), though the exact nuclei could not be reliably determined. This observation of pontine permeability in 0d and 3d repetitively injured animals is consistent with our data in the caudate, SNpr, SC, and CNIII/IV.

Subcortical regions including those analyzed here may be particularly biomechanically vulnerable to head rotation in the sagittal plane owing to the relationship between the center of mass of the brain and the center of rotation for the excursion. This relationship would be similar for rotation in the axial plane, but biomechanical loading distribution is predicted to differ for rotation in the coronal plane (for swine and other quadrupeds). In the coronal plane, stresses may be greater for peri-midline structures and trans-hemispheric connections may be more vulnerable. Therefore, future studies should explore the relationship between plane of head

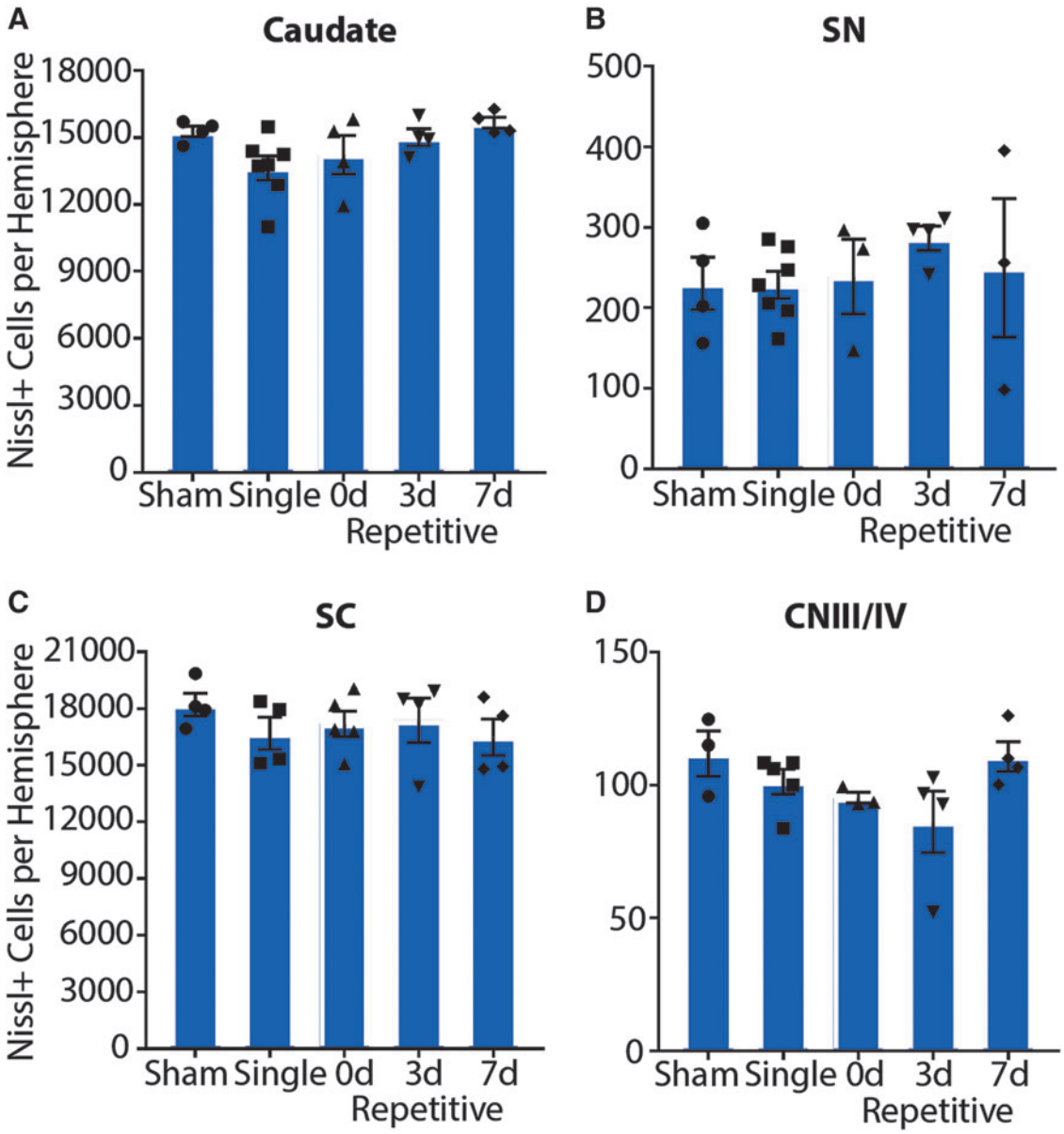

FIG. 7. Neuronal cell loss. There is no difference in the total number of Nissl+ cells in the **(A)** caudate, **(B)** SN, substantia nigra, **(C)** superior colliculus (SC), or **(D)** cranial nerve III/IV (CNIII/IV) between sham, single, or repetitively injured animals 15 min after injury. Error bars ± standard error of the mean. Color image is available online.

rotation and vulnerability of specific brain regions, especially those involved in clinically-relevant functional outcome measures such as control of eye movements.

In the present study of sagittal plane head rotation, increased oculomotor permeability was observed in 0d and 3d repetitively injured animals. In contrast to these groups, single and 7d repetitive injuries resulted in levels of permeability similar to sham injuries. The pathology associated with the spacing of these injuries is consistent with the literature examining the temporal window of vulnerability to repetitive injuries. For instance, a modified controlled cortical impact study (CCI) in mice found that 3- or 5-day repetitive injuries, but not single or 7-day repetitive injuries, led to significantly more behavioral dysfunction and, in the case of the 3-day repetitive group, increased axonal damage.[46] In another modified CCI study, mice injured repetitively 24 h apart had greater behavioral impairments and increased blood–brain barrier breakdown, axonal damage, and loss of MAP2 immunoreactivity than mice receiving a single injury.[47] Examination of temporal windows of vulnerability in large animal models has produced similar results. Using the same head rotational acceleration model employed in the current study, piglets were subjected to mild to moderate injuries in the axial plane once or repetitively 15 min apart,[48] or 24 h or 1 week apart.[49] While a moderate TBI separated by 15 min may not be a clinically relevant situation (or at a minimum would be extremely rare), we view this group in our study and others as a ''positive control'' for the acute biomechanical effects of repetitive TBI. Animals receiving mild repetitive injuries 15 min apart had increased foci of damaged axons compared with animals receiving a single injury. Piglets receiving moderate repetitive injuries 24 hours apart had increased mortality and injury severity (pathologically and behaviorally) compared with piglets receiving moderate repetitive

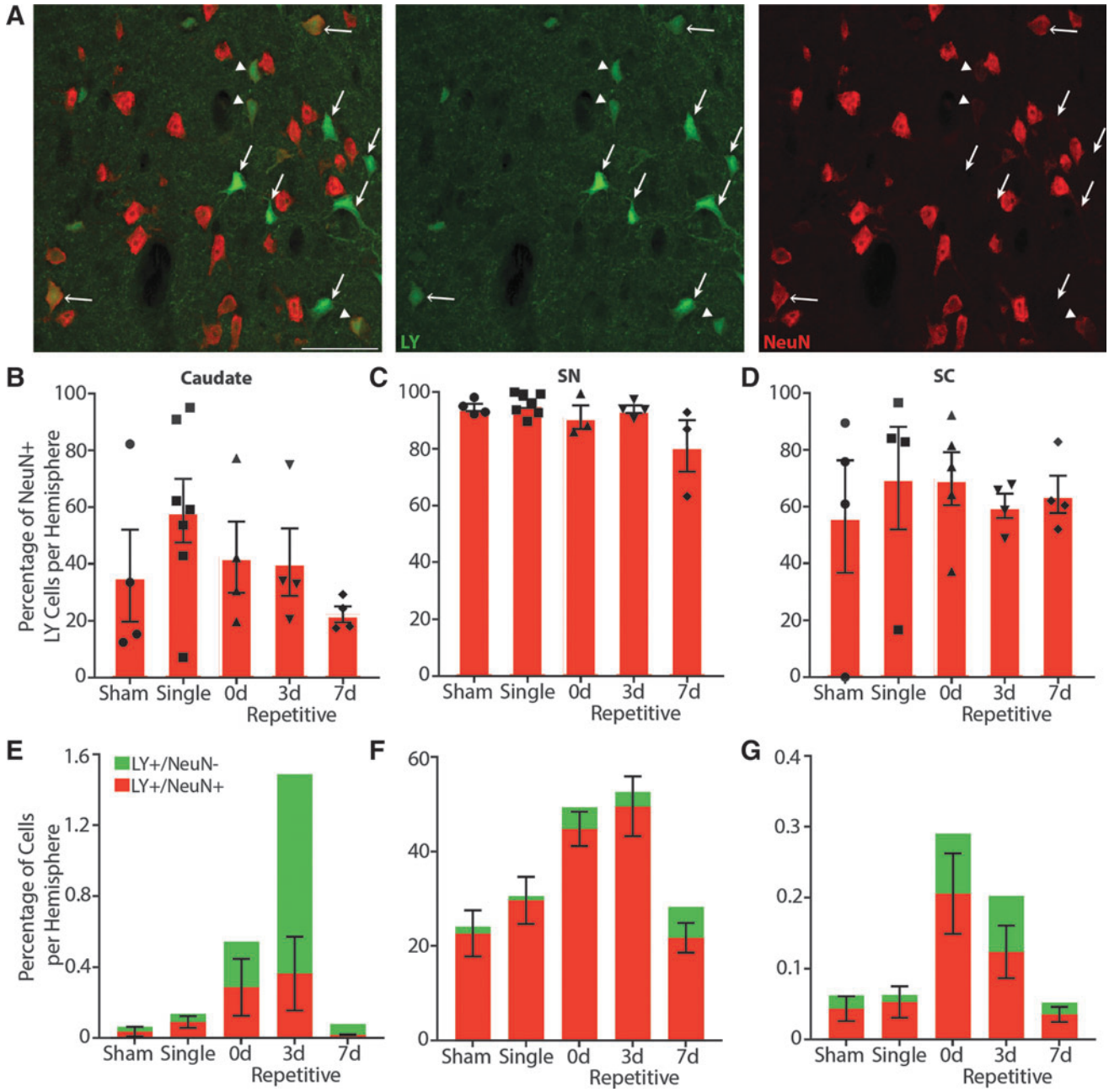

FIG. 8. Altered neuron-specific nuclear protein (NeuN) reactivity in permeabilized neurons. **(A)** Some Lucifer Yellow (LY)+ cells are NeuN+ (open arrows), while others have lost their NeuN signal (closed arrows). Other LY+ cells appear to have weakened NeuN reactivity (arrowheads). Representative image from caudate of 15 min (0d) repetitive injury. LY, green; NeuN, red. Scale bars = 50 μm. **(B-D)** Quantification of the percentage of permeabilized cells that were NeuN+ per hemisphere, ± standard error of the mean (SEM). There were no significant differences in LY+ NeuN loss between injury groups. Overall, only 42.46% of permeabilized cells were NeuN+ in the caudate, while 92.49% of substantia nigra (SN) and 64.48% of superior colliculus (SC) permeabilized cells were NeuN+. **(E-G)** Quantification of permeabilized cells with or without NeuN co-expression in context with the percentage of permeabilized cells per hemisphere, ± SEM. LY+/NeuN-, green; LY+/NeuN+, red. Both the caudate ($p = 0.0379$) and SC ($p = 0.0202$) displayed significant differences in the amount of LY+/NeuN- cells, but these differences were not significant in multiple comparison analyses. The substantia nigra pars reticulata (SNpr) displayed no significant differences in the number of LY+/NeuN- cells ($p = 0.1762$). Color image is available online.

injuries 7 days apart. Unlike the current study however, both 24 h and 7 days repetitive injuries produced poorer outcomes than single injuries.

Taken together with the results presented here, there appears to be increased vulnerability to damage from repeated TBI within 3 days of injury. We assessed other acute pathologies that could contribute to and/or be a consequence of this vulnerability, including neuronal cell loss, loss of NeuN antigenicity, and microglia reactivity. We did not observe cell loss in any areas, which is not surprising given that animals were sacrificed just 15 min after injury, while primary and secondary cell death are typically observed on a timescale ranging from hours to days or even weeks after TBI.[50]

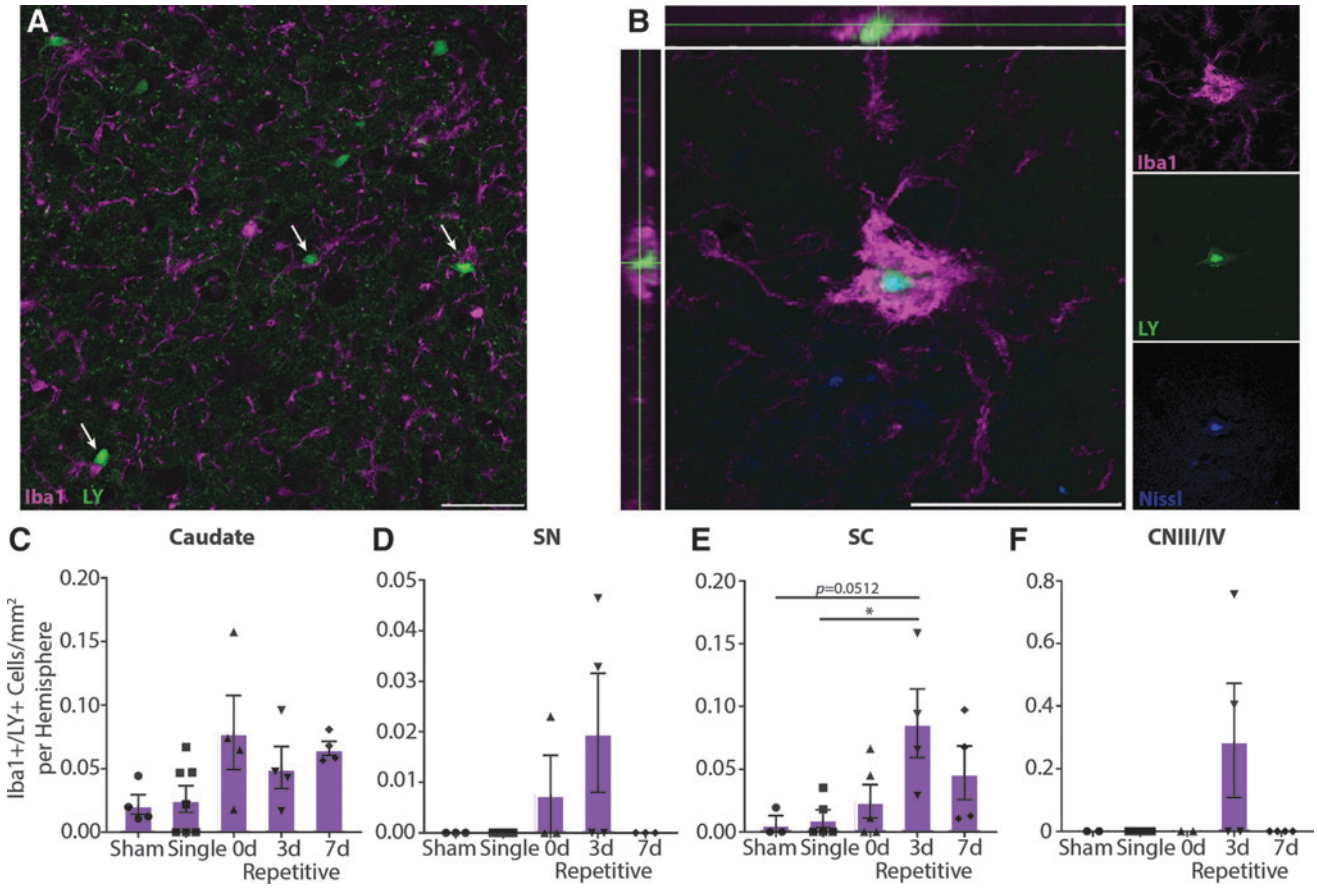

FIG. 9. Microglia interacting with permeabilized neurons. **(A)** In repetitively injured animals, microglia often contact Lucifer Yellow (LY)+ neurons (arrows). Representative image from caudate of 3-day (3d) repetitive injury. **(B)** Large microglia can be observed colocalized with LY+/Nissl+ cells, suggesting phagocytosis of permeabilized neurons. Representative image from caudate of 7-day (7d) repetitive injury. Iba1, purple; LY, green; Nissl, blue. Scale bars = 50 μm. **(C-F)** Quantification of large Iba1+ signal colocalized with LY, ± SEM. Phagocytosis occurs more frequently in repetitively injured animals, especially those injured 3 days apart, although these trends were only statistically significant in the superior colliculus (SC; caudate $p = 0.0680$; substantia nigra pars reticulata [SNpr] $p = 0.1457$; SC $p = 0.0273$; cranial nerve III/IV [CNIII/IV] $p = 0.2000$). Color image is available online.

NeuN is also frequently used as a marker for neuronal loss, although studies have shown that loss of NeuN signal may actually be due to injury-induced loss of antigenicity and could be used to predict delayed degeneration.[36,37] While we did not detect gross changes in total NeuN, we did observe that in some regions permeabilized cells frequently lost NeuN reactivity irrespective of injury group. This loss of NeuN in membrane-damaged neurons proportionately affects more cells in injuries that produce more permeability, such as those spaced repetitively 15 min or 3 days apart. This finding may indicate that more neurons in these animals will experience delayed cell death, although a recent study examining cortical neuronal membrane disruption at subacute and chronic time points (6 h to 4 weeks) following central fluid percussion injury (cFPI) in rats suggests that neuronal loss may not be the outcome.[51] Similar to the present work, after cFPI in rats there were no differences in the number of NeuN-negative cells between sham and injured animals, and membrane disruption was associated with loss of NeuN reactivity at 2 weeks after injury. However, there was no evidence of progression to cell death. Follow-up studies examining a longer-term cohort of animals will be necessary to determine the fate of neurons experiencing immediate and late membrane damage and the significance of alterations in NeuN expression over time.

Another contributor to vulnerability to damage could be changes in microglia. Overall microglia density and intensity did not differ between injury groups, which again may be due to the acute time frame after injury. We did note microglia contacting permeabilized neurons in all oculomotor regions, consistent with our earlier observations of increased microglia density in close proximity to permeabilized neurons after injury.[34] Further, we saw what appeared to be large microglia clusters completely surrounding LY+/Nissl+ neurons or debris, suggesting that we captured snapshots of microglia actively phagocytosing permeabilized neurons rapidly after injury. These cells were most often seen in repetitively injured animals, though the low frequency of these events and high variability across animals led to statistical significance only in the SC.

While we were limited to assessing acute pathologies 15 min after injury, increased vulnerability to damage from repetitive TBI could also be due to depletion of energetic reserves, pathological priming of cell death pathways, inflammation, and/or biomechanical stress-strain alterations in brain structure. Future studies should investigate these possible mechanisms. These findings could have important implications from a ''return to play'' perspective in competitive sports, so that the potential for damage from multiple concussions is minimized.

It should be noted that in our study of TBI-induced oculomotor vulnerability, we used female swine. In humans, girls have greater impairment on measures of vestibular-oculomotor function after sport-related concussion than boys,[52,53] and being female is associated with an increased likelihood of this dysfunction in pediatric populations.[54,55] In general, women are reported to experience more concussion-related symptoms and slower symptom resolution than men.[56] However, outcomes for males and females post-TBI appear to be dependent on the severity of injury and the types of outcomes measured, as well as whether the studies were conducted in animals or humans.[57] It is clear that more studies should include sex as a variable in order to determine differences in responses to injuries at the cellular/molecular and functional levels.

While more studies are examining the effect of sex on injury, to our knowledge no animal models have specifically examined oculomotor damage after TBI. A few animal studies have explored visual system pathology post-TBI using a variety of injury methods, although these have primarily focused on the retina and optic nerve/tract. For example, models employing impact acceleration,[58] cFPI,[59] and closed-head weight drop[60] have reported traumatic axonal injury along with inflammatory glial responses in the optic nerve/tract, lateral geniculate nucleus of the thalamus (LGN), and SC. Several rodent blast overpressure models of TBI have found retina and optic nerve/tract damage, as well as degenerating axon fibers and activated microglia in the LGN and SC.[61–64] Visual deficits after these blast injuries included reduced acuity and contrast sensitivity.[62,64] However, until now, oculomotor pathology has not been investigated.

The studies described above investigating visual system pathology following TBI have primarily focused on white matter injury. In contrast, the current work examined gray matter damage acutely after injury; in particular, neuronal plasma membrane permeability. Direct mechanical poration of neuronal plasma membranes due to injury has been well established both *in vitro*[4–8] and *in vivo*.[9,14,16,34,65-67] Importantly, studies using rodent TBI models of weight drop,[14] cFPI,[66] and CCI[9,16] to examine somatic changes in permeability have all demonstrated that mechanoporation is not a death sentence in all cases. Although some neurons display ultrastructural or enzymatic signs of cell death, others appear morphologically intact and are not positive for markers of necrosis or apoptosis. A study using fluorescent dextrans injected to the brain before and after injury showed that some cells were only labeled with the pre-injury dextran, indicating that they resealed.[14] Accordingly, in the present study LY is believed to mark cells that have resealed, as the dye would be washed out of unsealed cells during perfusion. Overall, these studies suggest that permeabilized neurons can survive the initial insult.

However, because the accompanying loss of osmotic and ionic homeostasis can disrupt normal cell function,[5,10–13] it is possible that these permeabilized neurons could contribute to dysfunction observed after TBI. Indeed, *in vitro* models of mechanical injury have shown increased plasma membrane permeability from shear stress resulted in electrophysiological disturbances,[7] while stretch injury resulted in disruption of neuronal network synchrony, loss of excitatory tone, and increased modular topology.[15] The dysfunction of permeabilized neurons in oculomotor regions could contribute to the insufficient activation observed in these nuclei in patients with mild TBI who experience deficits in saccades and vergence,[3] although further research is necessary to determine the precise role of permeabilized cells in the underlying mechanism(s) behind oculomotor dysfunction.

Conclusions

We have shown that repetitive closed-head diffuse TBI separated by 15 min or 3 days results in increased neuronal plasma membrane permeability in brain regions involved with oculomotor function. Despite the prevalence of oculomotor dysfunction after TBI, to our knowledge this is the first time that brain areas implicated in eye movements have been specifically examined for damage in a pre-clinical model. These neuronal plasma membrane disruptions and associated NeuN and microglia pathologies may mediate transient dysfunction and/or degeneration that may contribute to the oculomotor deficits following diffuse TBI. Overall, the presence of permeabilized neurons in oculomotor regions reveals the vulnerability of an eloquent sub-cortical circuit that may underlie a common clinical deficit associated with TBI. Future work will assess other types of longer-term damage in these areas, such as diffuse axonal injury, neuronal loss, inflammation, or synaptic changes. More importantly, we will examine whether damage in oculomotor regions translates to functional deficits in our swine model by assessing eye movements before and after rotational injuries.

Acknowledgments

The authors thank Dr. James P. Harris and Dr. Constance J. Mietus for technical contributions.

Funding Information

Financial support was provided by the Department of Veterans Affairs (RR&D Merit Review I01- RX001097 & BLR&D Merit Review I01-BX003748), the National Institutes of Health (U01-NS094340), the Department of Health of the Commonwealth of Pennsylvania (PA Consortium on TBI: PACT), and Penn's University Research Foundation. None of the funding sources aided in the collection, analysis, and interpretation of data; in the writing of the report; or in the decision to submit the paper for publication.

Author Disclosure Statement

No competing financial interests exist.

Supplementary Material

Supplementary Figure S1
Supplementary Figure S2
Supplementary Figure S3

References

1. Ciuffreda, K.J., Kapoor, N., Rutner, D., Suchoff, I.B., Han, M.E., and Craig, S. (2007). Occurrence of oculomotor dysfunctions in acquired brain injury: a retrospective analysis. Optometry 78, 155–161.
2. Goodrich, G.L., Flyg, H.M., Kirby, J.E., Chang, C.-Y., and Martinsen, G.L. (2013). Mechanisms of TBI and visual consequences in military and veteran populations. Optom. Vis. 90, 105–112.
3. Tyler, C.W., Likova, L.T., Mineff, K.N., and Nicholas, S.C. (2015). Deficits in the activation of human oculomotor nuclei in chronic traumatic brain injury. Front. Neurol. 6, 1–9.
4. Cullen, D.K., Vernekar, V.N., and LaPlaca, M.C. (2011). Trauma-induced plasmalemma disruptions in three-dimensional neural cultures are dependent on strain modality and rate. J. Neurotrauma 28, 2219–2233.
5. Geddes, D.M., LaPlaca, M.C., and Cargill, R.S. (2003). Susceptibility of hippocampal neurons to mechanically induced injury. Exp. Neurol. 184, 420–427.

6. Geddes, D.M., Cargill, R.S. 2nd, and LaPlaca, M.C. (2003). Mechanical stretch to neurons results in a strain rate and magnitude-dependent increase in plasma membrane permeability. J. Neurotrauma 20, 1039–1049.
7. LaPlaca, M.C., Prado, G.R., Cullen, D.K., and Irons, H.R. (2006). High rate shear insult delivered to cortical neurons produces heterogeneous membrane permeability alterations. Conf. Proc. IEEE Eng. Med. Biol. Soc. 2006, 2384–2387
8. LaPlaca, M.C., Prado, G.R., Cullen, D., and Simon, C.M. (2009). Plasma membrane damage as a marker of neuronal injury. Conf. Proc. IEEE Eng. Med. Biol. Soc. 2009, 1113–1116.
9. LaPlaca, M.C., Lessing, M.C., Prado, G.R., Zhou, R., Tate, C.C., Geddes-Klein, D., Meaney, D.F., and Zhang, L. (2019). Mechanoporation is a potential indicator of tissue strain and subsequent degeneration following experimental traumatic brain injury. Clin. Biomech. 64, 2–13.
10. LaPlaca, M.C., Lee, V.M., and Thibault, L.E. (1997). An in vitro model of traumatic neuronal injury: loading rate-dependent changes in acute cytosolic calcium and lactate dehydrogenase release. J. Neurotrauma 14, 355–368.
11. LaPlaca, M.C. and Thibault, L.E. (1998). Dynamic mechanical deformation of neurons triggers an acute calcium response and cell injury involving the N-methyl-D-aspartate glutamate receptor. J. Neurosci. Res. 52, 220–229.
12. Weber, J.T., Rzigalinski, B.A., Willoughby, K.A., Moore, S.F., and Ellis, E.F. (1999). Alterations in calcium-mediated signal transduction after traumatic injury of cortical neurons. Cell Calcium 26, 289–299.
13. McIntosh, T.K., Saatman, K.E., Raghupathi, R., Graham, D.I., Smith, D.H., Lee, V.M., and Trojanowski, J.Q. (1998). The Dorothy Russell Memorial Lecture. The molecular and cellular sequelae of experimental traumatic brain injury: pathogenetic mechanisms. Neuropathol. Appl. Neurobiol. 24, 251–267.
14. Farkas, O., Lifshitz, J., and Povlishock, J.T. (2006). Mechanoporation Induced by Diffuse Traumatic Brain Injury: An Irreversible or Reversible Response to Injury? J. Neurosci. 26, 3130–3140.
15. Patel, T.P., Ventre, S.C., and Meaney, D.F. (2012). Dynamic changes in neural circuit topology following mild mechanical injury in vitro. Ann. Biomed. Eng. 40, 23–36.
16. Whalen, M.J., Dalkara, T., You, Z., Qiu, J., Bermpohl, D., Mehta, N., Suter, B., Bhide, P.G., Lo, E.H., Ericsson, M., and Moskowitz, M.A. (2008). Acute plasmalemma permeability and protracted clearance of injured cells after controlled cortical impact in mice. J. Cereb. Blood Flow Metab. 28, 490–505.
17. Bailes, J.E., Dashnaw, M.L., Petraglia, A.L., and Turner, R.C. (2014). Cumulative effects of repetitive mild traumatic brain injury. Prog. Neurol. Surg. 28, 50–62.
18. Gardner, R.C. and Yaffe, K. (2015). Epidemiology of mild traumatic brain injury and neurodegenerative disease. Mol. Cell. Neurosci. 66, 75–80.
19. Gardner, R.C., Burke, J.F., Nettiksimmons, J., Goldman, S., Tanner, C.M., and Yaffe, K. (2015). Traumatic brain injury in later life increases risk for Parkinson disease. Ann. Neurol. 77, 987–995.
20. McKee, A.C., Cantu, R.C., Nowinski, C.J., Hedley-Whyte, E.T., Gavett, B.E., Budson, A.E., Santini, V.E., Lee, H.S., Kubilus, C.A., and Stern, R.A. (2009). Chronic traumatic encephalopathy in athletes: progressive tauopathy after repetitive head injury. J. Neuropathol. Exp. Neurol. 68, 709–735.
21. McKee, A.C. and Robinson, M.E. (2014). Military-related traumatic brain injury and neurodegeneration. Alzheimers. Dement. 10, S242–S53.
22. LoBue, C., Wilmoth, K., Cullum, C.M., Rossetti, H.C., Lacritz, L.H., Hynan, L.S., Hart, J.J., and Womack, K.B. (2016). Traumatic brain injury history is associated with earlier age of onset of frontotemporal dementia. J. Neurol. Neurosurg. Psychiatry 87, 817–820.
23. LoBue, C., Wadsworth, H., Wilmoth, K., Clem, M., Hart, J.J., Womack, K.B., Didehbani, N., Lacritz, L.H., Rossetti, H.C., and Cullum, C.M. (2017). Traumatic brain injury history is associated with earlier age of onset of Alzheimer disease. Clin. Neuropsychol. 31, 85–98.
24. Hikosaka, O., Takikawa, Y., and Kawagoe, R. (2000). Role of the basal ganglia in the control of purposive saccadic eye movements. Physiol. Rev. 80, 953–978.
25. Seger, C.A. (2013). The visual corticostriatal loop through the tail of the caudate: circuitry and function. Front. Syst. Neurosci. 7, 1–15.
26. Ross, D.T., Meaney, D.F., Sabol, M.K., Smith, D.H., and Gennarelli, T.A. (1994). Distribution of forebrain diffuse axonal injury following inertial closed head injury in miniature swine. Exp. Neurol. 126, 291–298.
27. Cullen, D.K., Harris, J.P., Browne, K.D., Wolf, J.A., Duda, J.E., Meaney, D.F., Margulies, S.S., and Smith, D.H. (2016). A porcine model of traumatic brain injury via head rotational acceleration. Methods Mol. Biol. 1462, 289–324
28. Bailey, E.L., McCulloch, J., Sudlow, C., and Wardlaw, J.M. (2009). Potential animal models of lacunar stroke: a systematic review. Stroke 40, e451–e458.
29. Howells, D.W., Porritt, M.J., Rewell, S.S.J., O'Collins, V., Sena, E.S., van der Worp, H.B., Traystman, R.J., and Macleod, M.R. (2010). Different strokes for different folks: the rich diversity of animal models of focal cerebral ischemia. J. Cereb. Blood Flow Metab. 30, 1412–1431.
30. Zhang, K. and Sejnowski, T.J. (2000). A universal scaling law between gray matter and white matter of cerebral cortex. Proc. Natl. Acad. Sci. U. S. A. 97, 5621–5626.
31. Smith, D.H., Chen, X.H., Xu, B.N., McIntosh, T.K., Gennarelli, T.A., and Meaney, D.F. (1997). Characterization of diffuse axonal pathology and selective hippocampal damage following inertial brain trauma in the pig. J. Neuropathol. Exp. Neurol. 56, 822–834.
32. Smith, D., Chen, X., Nonaka, M., Trojanowski, J., Lee, V., Saatman, K., Leoni, M., Xu, B., Wolf, J., and Meaney, D. (1999). Accumulation of amyloid beta and tau and the formation of neurofilament inclusions following diffuse brain injury in the pig. J. Neuropathol. Exp. Neurol. 58, 982–992.
33. Browne, K.D., Chen, X.H., Meaney, D.F., and Smith, D.H. (2011). Mild traumatic brain injury and diffuse axonal injury in Swine. J. Neurotrauma 28, 1747–1755.
34. Wofford, K.L., Harris, J.P., Browne, K.D., Brown, D.P., Grovola, M.R., Mietus, C.J., Wolf, J.A., Duda, J.E., Putt, M.E., Spiller, K.L., and Cullen, D.K. (2017). Rapid neuroinflammatory response localized to injured neurons after diffuse traumatic brain injury in swine. Exp. Neurol. 290, 85–94.
35. Folkerts, M.M., Berman, R.F., Muizelaar, J.P., and Rafols, J.A. (1998). Disruption of MAP-2 immunostaining in rat hippocampus after traumatic brain injury. J. Neurotrauma 15, 349–363.
36. Unal-Cevik, I., Kilinc, M., Gursoy-Ozdemir, Y., Gurer, G., and Dalkara, T. (2004). Loss of NeuN immunoreactivity after cerebral ischemia does not indicate neuronal cell loss: a cautionary note. Brain Res. 1015, 169–174.
37. Collombet, J.M., Masqueliez, C., Four, E., Burckhart, M.F., Bernabe, D., Baubichon, D., and Lallement, G. (2006). Early reduction of NeuN antigenicity induced by soman poisoning in mice can be used to predict delayed neuronal degeneration in the hippocampus. Neurosci. Lett. 398, 337–342.
38. Sommer, C., Straehle, C., Koethe, U., and Hamprecht, F.A. (2011). Ilastik: Interactive learning and segmentation toolkit, in: *2011 IEEE International Symposium on Biomedical Imaging: From Nano to Macro.* Chicago, IL, pps. 230–233.
39. Hikosaka, O., Sakamoto, M., and Usui, S. (1989). Functional properties of monkey caudate neurons I . Activities related to saccadic eye movements. J. Neurophysiol. 61, 780–798.
40. Huerta, M.F., and Kaas, J.H. (1990). Supplementary eye field as defined by intracortical microstimulation: connections in macaques. J. Comp. Neurol. 293, 299–330.
41. Stanton, G.B., Goldberg, M.E., and Bruce, C.J. (1988). Frontal eye field efferents in the macaque monkey: I. Subcortical pathways and topography of striatal and thalamic terminal fields. J. Comp. Neurol. 271, 473–492.
42. Updyke, B. V. (1993). Organization of visual corticostriatal projections in the cat, with observations on visual projections to claustrum and amygdala. J. Comp. Neurol. 327, 159–193.
43. Royce, G.J. and Laine, E.J. (1984). Efferent connections of the caudate nucleus, including cortical projections of the striatum and other basal ganglia: an autoradiographic and horseradish peroxidase investigation in the cat. J. Comp. Neurol. 226, 28–49.
44. May, P.J. (2014). Superior colliculus, in: *Encyclopedia of Neuroscience, Second Ed.* Springer: Berlin, Heidelberg, 351–354.
45. Mani, R., Asper, L., and Khuu, S.K. (2018). Deficits in saccades and smooth-pursuit eye movements in adults with traumatic brain injury: a systematic review and meta-analysis. Brain Inj. 32, 1315–1336.

46. Longhi, L., Saatman, K.E., Fujimoto, S., Raghupathi, R., Meaney, D.F., Davis, J., McMillan, A., Conte, V., Laurer, H.L., Stein, S., Stocchetti, N., and McIntosh, T.K. (2005). Temporal window of vulnerability to repetitive experimental concussive brain injury. Neurosurgery 56, 364–373.
47. Laurer, H.L., Bareyre, F.M., Lee, V.M.Y.C., Trojanowski, J.Q., Longhi, L., Hoover, R., Saatman, K.E., Raghupathi, R., Hoshino, S., Grady, M.S., and McIntosh, T.K. (2001). Mild head injury increasing the brain's vulnerability to a second concussive impact. J. Neurosurg. 95, 859–870.
48. Raghupathi, R., Mehr, M.F., Helfaer, M.A., and Margulies, S.S. (2004). Traumatic axonal injury is exacerbated following repetitive closed head injury in the neonatal pig. J. Neurotrauma 21, 307–316.
49. Friess, S.H., Ichord, R.N., Ralston, J., Ryall, K., Helfaer, M.A., Smith, C., and Margulies, S.S. (2009). Repeated traumatic brain injury affects composite cognitive function in piglets. J. Neurotrauma 26, 1111–1121.
50. Raghupathi, R., Graham, D.I., and McIntosh, T.K. (2000). Apoptosis after traumatic brain injury. J. Neurotrauma 17.
51. Hernandez, M.L., Chatlos, T., Gorse, K.M., and Lafrenaye, A.D. (2019). Neuronal membrane disruption occurs late following diffuse brain trauma in rats and involves a subpopulation of NeuN negative cortical neurons. Front. Neurol. 10, 1–13.
52. Henry, L.C., Elbin, R.J., Collins, M.W., Marchetti, G., and Kontos, A.P. (2016). Examining recovery trajectories after sport-related concussion with a multimodal clinical assessment approach. Neurosurgery 78, 232–240.
53. Sufrinko, A.M., Mucha, A., Covassin, T., Marchetti, G., Elbin, R.J., and Collins, M.W. (2017). Sex differences in vestibular/ocular and neurocognitive outcomes after sport-related concussion. Clin. J. Sport Med. 27, 133–138.
54. Ellis, M.J., Cordingley, D.M., Vis, S., Reimer, K.M., Leiter, J., and Russell, K. (2017). Clinical predictors of vestibulo-ocular dysfunction in pediatric sports-related concussion. J. Neurosurg. Pediatr. 19, 38–45.
55. Womble, M.N., McAllister-Deitrick, J., Marchetti, G.F., Reynolds, E., Collins, M.W., Elbin, R.J., and Kontos, A.P. (2019). Risk factors for vestibular and oculomotor outcomes after sport-related concussion. Clin. J. Sport Med. 00, 1.
56. Zuckerman, S.L., Apple, R.P., Odom, M.J., Lee, Y.M., Solomon, G.S., and Sills, A.K. (2014). Effect of sex on symptoms and return to baseline in sport-related concussion: Clinical article. J. Neurosurg. Pediatr. 13, 72–81.
57. Gupte, R., Brooks, W., Vukas, R., Pierce, J., and Harris, J. (2019). Sex differences in traumatic brain injury: what we know and what we should know. J. Neurotrauma 29, 1–29.
58. Xu, L., Nguyen, J. V., Lehar, M., Menon, A., Rha, E., Arena, J., Ryu, J., Marmarou, N.M.-A.C.R., and Koliatsos, V.E. (2016). Repetitive mild traumatic brain injury with impact acceleration in the mouse: Multifocal axonopathy, neuroinflammation, and neurodegeneration in the visual system. Exp. Neurol. 275, 436–449.
59. Wang, J., Hamm, R.J., and Povlishock, J.T. (2011). Traumatic axonal injury in the optic nerve: evidence for axonal swelling, disconnection, dieback, and reorganization. J. Neurotrauma 28, 1185–1198.
60. Evanson, N.K., Guilhaume-Correa, F., Herman, J.P., and Goodman, M.D. (2018). Optic tract injury after closed head traumatic brain injury in mice: A model of indirect traumatic optic neuropathy. PLoS One 13, 1–20.
61. DeMar, J., Sharrow, K., Hill, M., Berman, J., Oliver, T., and Long, J. (2016). Effects of primary blast overpressure on retina and optic tract in rats. Front. Neurol. 7, 1–12.
62. Guley, N.H., Rogers, J.T., Mar, N.A. Del, Deng, Y., Islam, R.M., D'Surney, L., Ferrell, J., Deng, B., Hines-Beard, J., Bu, W., Ren, H., Elberger, A.J., Marchetta, J.G., Rex, T.S., Honig, M.G., and Reiner, A. (2016). A novel closed-head model of mild traumatic brain injury using focal primary overpressure blast to the cranium in mice. J. Neurotrauma FEB 15, 403–422.
63. Petras, J.M., Bauman, R.A., and Elsayed, N.M. (1997). Visual system degeneration induced by blast overpressure. Toxicology 121, 41–49.
64. Reiner, A., Heldt, S.A., Presley, C.S., Guley, N.H., Elberger, A.J., Deng, Y., D'Surney, L., Rogers, J.T., Ferrell, J., Bu, W., Del Mar, N., Honig, M.G., Gurley, S.N., and Moore, B.M. (2015). Motor, visual and emotional deficits in mice after closed-head mild traumatic brain injury are alleviated by the novel CB2 inverse agonist SMM-189. Int. J. Mol. Sci. 16, 758–787.
65. Pettus, E.H., Christman, C.W., Giebel, M.L., and Povlishock, J.T. (1994). Traumatically induced altered membrane permeability: its relationship to traumatically induced reactive axonal change. J. Neurotrauma 11, 507–522.
66. Singleton, R.H. and Povlishock, J.T. (2004). Identification and characterization of heterogeneous neuronal injury and death in regions of diffuse brain injury: evidence for multiple independent injury phenotypes. J. Neurosci. 24, 3543–3553.
67. Stone, J.R., Okonkwo, D.O., Dialo, A.O., Rubin, D.G., Mutlu, L.K., Povlishock, J.T., and Helm, G.A. (2004). Impaired axonal transport and altered axolemmal permeability occur in distinct populations of damaged axons following traumatic brain injury. Exp. Neurol. 190, 59–69.

Address correspondence to:
D. Kacy Cullen, PhD
University of Pennsylvania
3320 Smith Walk, 105E Hayden Hall
Philadelphia, PA 19104
USA

E-mail: dkacy@pennmedicine.upenn.edu